ISTITUTO NAZIONALE DI FISICA NUCLEARE

Sezione di Genova

INFN/TC–94/05
22 Aprile 1994

R. De Lorenzi, P. Fabbricatore, S. Farinon, G. Gemme, R. Musenich, R. Parodi, S. Pepe and B. Zhang:

STATUS REPORT OF THE INFN R&D ACTIVITIES FOR Al-STABILISED CONDUCTORS OF LARGE MAGNETS FOR LHC DETECTORS

Servizio Documentazione
dei Laboratori Nazionali di Frascati

INFN – Istituto Nazionale di Fisica Nucleare
Sezione di Genova

INFN/TC–94/05
26 Aprile 1994

STATUS REPORT OF THE INFN R&D ACTIVITIES FOR Al-STABILISED CONDUCTORS OF LARGE MAGNETS FOR LHC DETECTORS

R. De Lorenzi, P. Fabbricatore, S. Farinon, G. Gemme, R. Musenich, R. Parodi, S. Pepe and B. Zhang

INFN – Sezione di Genova, Via Dodecaneso 33, I-16146, Genova, Italy

ABSTRACT

In this paper we report on the activities of INFN Genova in the development of conductors for LHC detector magnets. Part of this work is co-ordinated by the MAG collaboration including CERN, SACLAY, RAL and other European laboratories. The two main activities of the INFN Genova magnet group are the development of the experimental techniques for the cable characterisation and the stability studies, with a special attention to the problems related to CMS solenoid. The experimental activities were devoted to the development of a sample holder for critical current measurements of Al-stabilised conductors up to 4.5 T and a current of about 10 kA. These measurements were carried on a cable for the magnet of ALEPH detector at CERN (LEP), because it was the only available conductor. With relation to stability, we show that a general 3-D code for transient thermal analysis can be used to calculate the minimum energy required to have a quench propagation (*MPE*) in a winding with an aluminium stabilised conductor. It is only required to improve the code with a suitable routine for the heat generation calculation including the current sharing and the finite magnetic diffusion.

1. - INTRODUCTION

The magnets at the moment under design for the Large Hadron Collider detectors at CERN, ATLAS and CMS, are based on Al stabilised conductors [1,2]. These magnets are big indirectly cooled structures so that the stability against thermal disturbances is a critical point. Stability leads two different problems:

- What is the amount of energy dissipated in the winding as thermal disturbances ?
- What is the minimum energy, which can be dissipated without causing a quench ?

The answer to the first question can be find only through a specific experimental activity, aiming to reproduce some typical situations of a conductor placed in a winding. In this paper such a problem is not studied.

Our activity was directed to the second question, about the possibility to make a prevision of the Minimum Energy for a Quench Propagation (*MPE*) or the Minimum Propagating Zone (*MPZ*).

An answer to both the questions is indeed necessary to proceed towards a correct magnet design, which should optimise the winding structure minimising the possibility of heat releases and maximising the *MPE*. Our work can be considered the first step towards this target.

The problem to determine the *MPE* was formulated as follows:

For a given homogeneous and anisotropic winding structure, a given energy is released as heat inside the winding. Is a normal zone generated? Does the normal zone propagate?

In order to answer to these questions we followed two different approaches:

1) Experimental approach. A sample holder was designed and constructed. Inside the sample holder the conductor of ALEPH magnet was wound in one turn geometry. This structure was used for stability measurements as well as for critical current measurements.

2) Computational approach. One dimensional thermal transient code was developed including the special heat generation of a superconducting to normal transition. The heat generation routine was then included in an existing 3-D code (HEATING). The 1-D and 3-D codes were tested simulating simple structures and comparing the results with a further 3-D code (ANSYS). The modified version of HEATING was then used to simulate the response to a disturbance of the ALEPH conductor.

2. - NUMERICAL APPROACH TO STABILITY

2.1. - Heat Conduction Equation

The heat conduction equation in a homogeneous and anisotropic medium can be generally written [3,4] as:

$$\frac{\partial}{\partial x}k_x\frac{\partial}{\partial x}T(\vec{r},t)+\frac{\partial}{\partial y}k_y\frac{\partial}{\partial y}T(\vec{r},t)+\frac{\partial}{\partial z}k_z\frac{\partial}{\partial z}T(\vec{r},t)=$$
$$=C(\vec{r},T)\frac{\partial T(\vec{r},t)}{\partial t}+\dot{G}(\vec{r},T,t)+\dot{G}_d(\vec{r},T,t)-\dot{H}(\vec{r},T,t) \qquad (1)$$

where $T(\vec{r},t)$ is the temperature at the position r=r(x,y,z) and time t, k is the thermal conductivity , C the specific heat , $\dot{G}(T,\vec{r},t)$ is the heat generation, in our case due to Joule effect, $\dot{G}_d(T,\vec{r},t)$ is the external disturbance, $\dot{H}(T,\vec{r},t)$ is a generic term of heat transfer including radiation or transfer to a LHe bath.

In our case, since the system is divided into elements of dimension Δx, Δy, and Δz (see fig.1) eq. (1) can be re-written for each node *i* as:

$$C_i\frac{T_i^{n+1}-T_i^n}{\Delta t}=P_i^n+\sum_{m=1}^{6}K_m^i\left(T_m^n-T_i^n\right) \qquad (2)$$

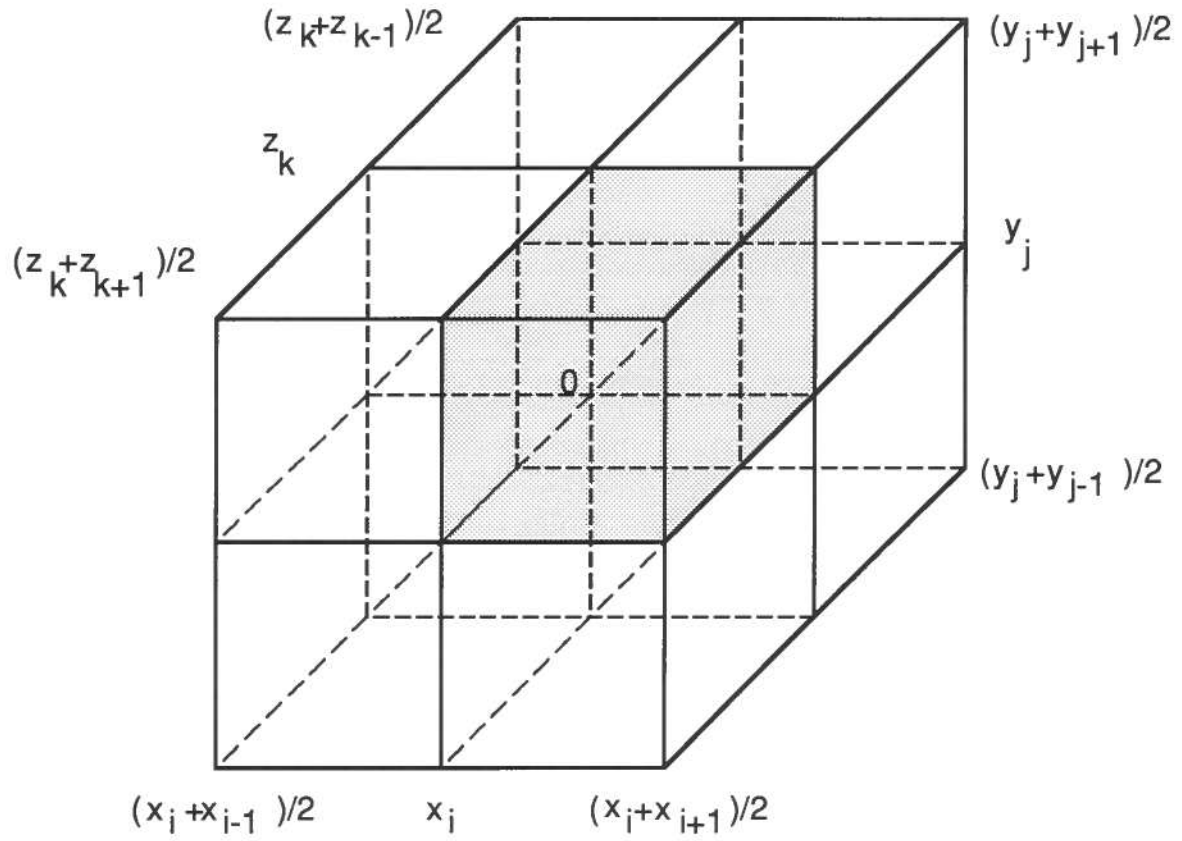

FIG. 1 - Element of volume related to a generic node 0.

The element can be divided into 8 octants , each having a volume V_j

where T_m^n is the temperature of the m-th node close to the node i at time t_n, i.e. after the n-th time step Δt ; $K_{i,m}$ is the thermal conductivity between nodes i and m ; C_i is the thermal capacity of the material related to node i; P_i^n is the heat generation in i at time t_n, including both $\dot{G}_d$ and $\dot{G}$.

For a 3-D problem at time t_n we need for each node one value of C_i and P_i and six values of $K_{i,m}$, calculated according to :

$$C_i = \sum_{j=1}^{8} C_{Pj}\rho_j V_j \tag{3a}$$

$$P_i^n = \sum_{j=1}^{8} Q_j^n V_j \tag{3b}$$

$$K_m^i = \frac{1}{L_{i,m}} \sum_{\xi=1}^{4} k_{m,\xi} A_{m,\xi} \tag{3c}$$

where :

V_j: Volume of j-th octant relative to node i (in m^3) (dark region in fig.1)
C_{Pj}: Specific heat of material in octant j (in J Kg^{-1} K^{-1})
ρ_j: Density of material in octant j (in Kg m^{-3})
Q_j^n: Heat generation per unit volume at time t_n in octant j (in Watt m^{-3})
$L_{i,m}$: Distance between nodes i and m (in m)
$k_{m,\xi}$: Thermal conductivity of material through the ξ-th path, among 4, between the nodes i and m (in Watt m^{-1} K^{-1})
$A_{m,\xi}$: Cross section normal to the ξ-th path, among 4, between the nodes i and m (in m^2)

The system defined by eq.2 allows to calculate the temperature distribution for all the nodes i at the time t_{n+1}, once the temperature distribution is known at time t_n. It is necessary to know the temperature distribution at time t=0. eq.2 can be written in a more general form, also valid for 1-D or 2-D problems, introducing M_i the number of the nearest nodes to node i and α_m the m-th node next to node i:

$$C_i \frac{T_i^{n+1} - T_i^n}{\Delta t} = P_i^n + \sum_{m=1}^{M_i} K_{\alpha m}^i \left(T_{\alpha m}^n - T_i^n\right) \tag{4}$$

2.2. - Numerical Methods

In this section we briefly recall the standard numerical methods, which are used to solve the heat conduction equation.

One of the most used method is the *Classic Explicit Procedure (CEP)* , based on eq.4. The temperature at time t_{n+1} can be written as :

$$T_i^{n+1} = T_i^n + \frac{\Delta t}{C_i}\left[P_i^n + \sum_{m=1}^{M_i} K_{\alpha m}^i \left(T_{\alpha m}^n - T_i^n\right)\right] \tag{5}$$

Using this method, a critical parameter is the time step Δt . In order to avoid a heat flow from a node i to a node m with $T_m > T_i$, the time step should fulfil the following condition:

$$\Delta t \leq \min_{i \geq 1}\left(\frac{C_i}{\sum_{m=1}^{M_i} K_{\alpha m}^i}\right) \tag{6}$$

For stability problems of pure aluminium structures at low temperature the time step could have a very low value. In fact at T=10 K and using elements of 1 cm^3 we find $\Delta t = 10^{-5}$ s, a value which implies too long numerical calculation. This problem can be partly solved if eq. 5 is re-written as:

$$T_i^{n+1} = T_i^n + \frac{1}{1+Z_i}\left\{\frac{\Delta t}{C_i}\left[P_i^n + \sum_{m=1}^{M_i} K_{\alpha m}^i \left(T_{\alpha m}^n - T_i^n\right)\right] + Z_i\left[T_i^n - T_i^{n-1}\right]\right\} \tag{7}$$

where :

$$Z_i = \begin{cases} 0 & \text{if } \dfrac{\Delta t}{(\Delta t_{max})_i} \leq 1 \\ 0.5\left[\dfrac{\Delta t}{(\Delta t_{max})_i} - 1\right] & \text{if } \dfrac{\Delta t}{(\Delta t_{max})_i} > 1 \end{cases} \tag{8}$$

$(\Delta t_{max})_i$ is the maximum allowed time step for the node i according to eq.6. The general rule is that the accuracy of the calculation is good if $Z_i = 0$ for at least half the nodes [5].

If the right side of eq.5 is calculated at the time t_{n+1} instead that at time t_n, the numerical technique is called *Classic Implicit Procedure (CIP)*. If the right side is calculated at an intermediate time between t_{n+1} and t_n, we have the *Cranck-Nicolson Procedure*.[6]. Both these methods do not calculate the temperature writing an equation for each node, but rather a system

of equations is written, with the number of equations equal to the number of nodes. These methods are based on a parameter Θ such that :

$$C_i^{n+\Theta}\frac{T_i^{n+1}-T_i^n}{\Delta t}=P_i^{n+\Theta}+\Theta\left[\sum_{m=1}^{M_i}{}_iK_{\alpha m}^{n+\Theta}\left(T_{\alpha m}^{n+1}-T_i^{n+1}\right)\right]+ \\ +(1-\Theta)\left[\sum_{m=1}^{M_i}{}_iK_{\alpha m}^{n+\Theta}\left(T_{\alpha m}^{n}-T_i^{n}\right)\right] \tag{9}$$

If Θ=0, eq. 9 represents the *CEP*, if Θ=0.5 we have the *Cranck Nicolson Procedure*, if Θ=1 we have the *CIP*.

For a system with N nodes, eq.9 represents a system of N equations, which can be written as:

$$-\Theta\left[\sum_{m=1}^{M_i}{}_iK_{\alpha m}^{n+\Theta}T_{\alpha m}^{n+1}\right]+\left[\frac{C_i^{n+\Theta}}{\Delta t}+\Theta\sum_{m=1}^{M_i}{}_iK_{\alpha m}^{n+\Theta}\right]T_i^{n+1}=H_i \tag{10}$$

where:

$$H_i=\frac{C_i^{n+\Theta}}{\Delta t}T_i^n+P_i^{n+\Theta}+(1-\Theta)\left[\sum_{m=1}^{M_i}{}_iK_{\alpha m}^{n+\Theta}\left(T_{\alpha m}^{n}-T_i^{n}\right)\right] \tag{11}$$

Defining:

$$D_i=\frac{C_i^{n+\Theta}}{\Delta t}+\Theta\sum_{m=1}^{M_i}{}_iK_{\alpha m}^{n+\Theta}, \tag{12}$$

and omitting the index n+1 of the temperature T, eq.10 becomes:

$$-\Theta\left[\sum_{m=1}^{M_i}{}_iK_{\alpha m}^{n+\Theta}T_{\alpha m}\right]+D_iT_i=H_i \tag{13}$$

Solving the temperature:

$$T_i=\frac{\Theta\left[\sum_{m=1}^{M_i}{}_iK_{\alpha m}^{n+\Theta}T_{\alpha m}\right]+H_i}{D_i} \tag{14}$$

eq. 14 can be solved by an iterative method until a convergence for the temperature distribution is found.

2.3. - Application of numerical methods to stability problems.

For a stability problem of superconducting cables or windings, a general thermal code including transient analysis can be used. The only characteristic point is the heat generation, which should include the particular features of a superconducting to normal transition. These features are the current sharing and the finite magnetic diffusivity of the stabiliser, as we will discuss in the next section. Our approach to stability can be schematised by the following points:

1 - A simple home made 1-D FORTRAN code, which includes the heat generation routine, was developed. The numerical *CEP* technique was used. Our aim was to prepare the heat generation routine to be inserted in a more general 3-D code.

2 - The code HEATING[4], developed in Oak Ridge Laboratories, was acquired and implemented on an ALPHA-VAX computer. The developed heat generation routine was included in the code source.

3 - A general 3-D code for thermal analysis (ANSYS) was also used in order to understand whether a non-specialist code can give satisfactory answers to stability problems .

The three codes were compared analysing a simple 1-D system. Starting from this comparison we were able to decide about the code to be used for 3-D analysis. In the next sections these points are discussed in details.

3. - HEAT GENERATION

The heat generation should include the two main features of a superconducting to normal transition, i.e. the current sharing and the finite magnetic diffusivity. The current sharing is a classical problem [7,8] for composite conductor. As represented in fig.2, the critical current at fixed dc magnetic field is supposed to be a linear function of the temperature. At a fixed current I_m, it exists a temperature $T_g = \frac{I_m}{I_{c0}} T_c(I=0)$, at which I_m is the critical current. For temperatures higher than T_g and lower than $T_c(I=0)$, the current is shared between the matrix and the superconductor.

The power dissipation can be written as

$$\dot{G} = \lambda J_m E = \frac{\lambda^2 J_m \rho [J_m - J_c(T)]}{1-\lambda}, \qquad (15)$$

where λ is the superconducting to normal ratio, J_m is the transport current divided by the cross section of the superconductor, E is the electric field and ρ is the matrix resistivity. Since

$$J_m - J_c(T) = J_m \frac{T - T_g}{T_c - T_g} \tag{16}$$

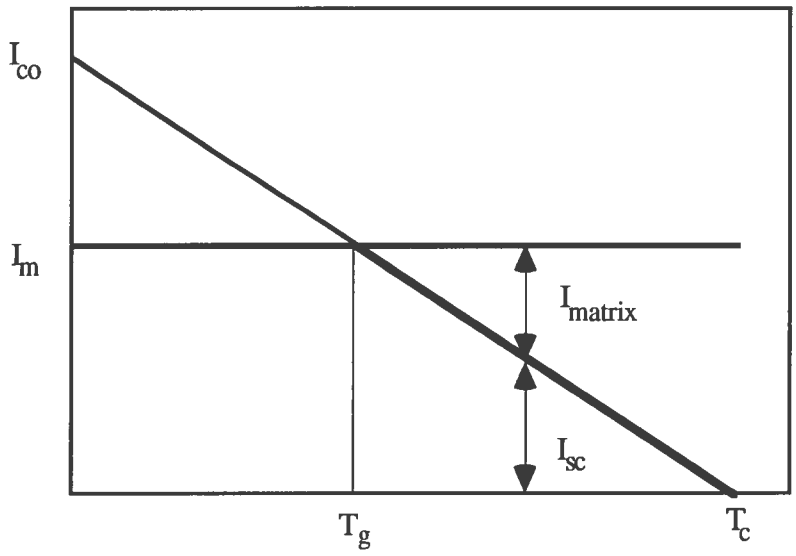

FIG. 2 - Current sharing in a composite conductor

we obtain for the power dissipation:

$$\dot{G} = \frac{\lambda^2 J_m^2 \rho}{1-\lambda} \frac{T - T_g}{T_c - T_g} = \dot{G}_c \frac{T - T_g}{T_c - T_g}. \tag{17}$$

eq.17 is valid if the current is immediately distributed in the whole cross section of the matrix. For large conductor of pure aluminium, eq.17 can not be applied.

Both the thermal and electrical processes can be described by a diffusion equation:

$$\begin{aligned} D_T \nabla^2 T &= \partial T / \partial t \\ D_m \nabla^2 \vec{J} &= \partial \vec{J} / \partial t \end{aligned} \tag{18}$$

where D_T and D_m are the thermal and magnetic diffusion coefficients:

$$D_T = \frac{k}{\gamma C} \tag{19.a}$$

$$D_m = \frac{\rho}{\mu_0} \tag{19.b}$$

For pure aluminium (99.99%) at T=10 K , we obtain:

$$D_m \sim 10^{-5}\ m^2 s^{-1}$$

$$D_T \sim 10^{-3}\ m^2 s^{-1}$$

This means that the current diffusion in the aluminium cross section occurs with a characteristic time much higher than the time for thermal diffusion, so that if a normal zone develops, the current is not transferred to the whole matrix, but only to a small area close to the superconducting strands. Therefore heat generation is much higher with respect to the one related to instantaneous current distribution, being much higher the current densities.

To calculate the new form for the heat generation in the stabiliser, the current diffusion equation has been solved.

Let's suppose one dimensional diffusion process across the stabiliser.

The current diffusion equation is:

$$\frac{\partial^2 J(x,t)}{\partial x^2} = \frac{1}{D_m}\frac{\partial J(x,t)}{\partial t} \tag{20}$$

with the appropriate boundary conditions:

$$\frac{\partial J}{\partial x}(x = 0, t) = 0 \tag{21a}$$

$$\int_A J\, dA = I \tag{21b}$$

and:

$$J(x, t = 0) = \begin{cases} J_0 & 0 \le x \le d \\ 0 & d < x < L \end{cases} \tag{21c}$$

where A is total cross section and J_0 is the current I divided the superconductor area.

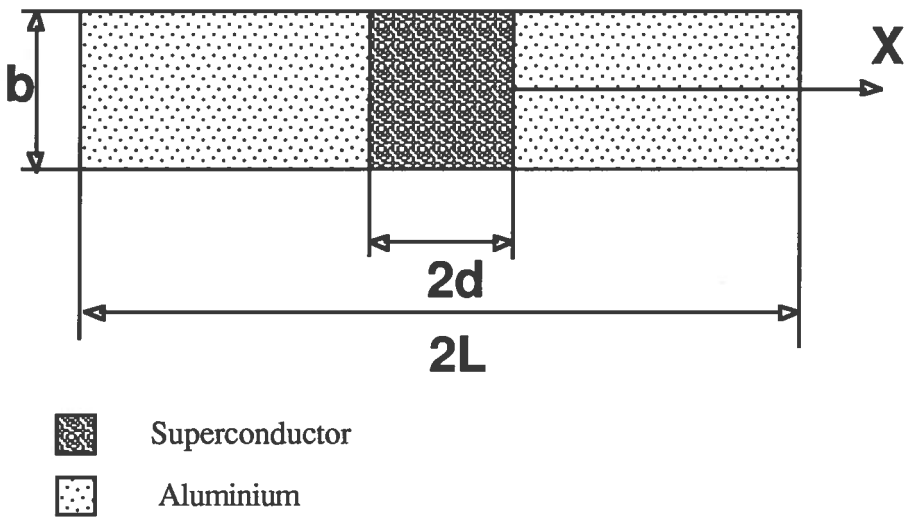

FIG. 3 - Schematic modelling for 1-D current diffusion problem

The solution of eq.20 , with the conditions (21a), (21b), (21c) is [9]:

$$J(x,t) = \frac{I}{2bd}\sum_{n=1}^{\infty}\frac{2}{n\pi}\sin(\beta_n d)\cos(\beta_n x)e^{-D_m\beta_n^2 t} + \frac{I}{2bL} \qquad (22)$$

where $\beta_n = \frac{n\pi}{L}$. Fig.4 shows the current distribution calculated for the ALEPH conductor (I=5.0 kA); the values of current densities are normalised to the value of the current density uniformly distributed across the stabiliser ($J_{uniform}$).

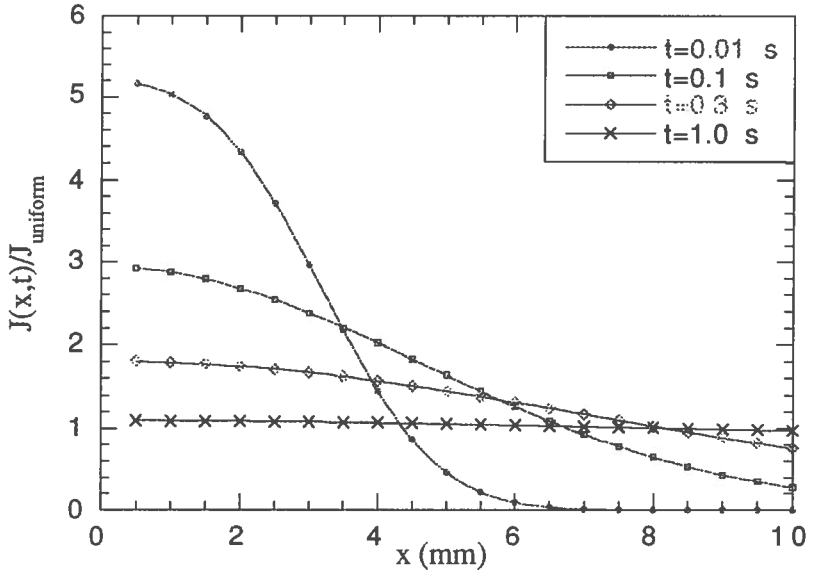

FIG.4 - Current density distribution in the stabiliser at different times for ALEPH conductor at I=5 kA and B=2 T

The heat generation including both sharing and current diffusion effect can be calculated.

The total power generated in the normal zone is given by:

$$W = R_{Al} I_{Al}^2 + R_{SC} I_C^2 \tag{23}$$

the heat generation consequently is:

$$\dot{G}(x,t,T) = (1-\lambda)\rho_{Al} J_{Al}^2(x,t,T) + \lambda \rho_{SC} J_C^2(T) \tag{24}$$

where λ is the superconducting to normal ratio (or "filling factor"). Averaging over the whole cross section of the conductor:

$$\dot{G}(T,t) = (1-\lambda) q_a(T,t) + \lambda \rho_{Al} J_{Al}(T,t)_{|x=d} J_C(T) \tag{25}$$

where:

$$q_a(t) = \frac{\rho I^2}{2(2bd)^2} \sum_{n=1}^{\infty} \left[\frac{2}{n\pi} \sin(\beta_n d) e^{-D_m \beta_n^2 t} \right]^2 + \frac{\rho I^2}{2(2bL)^2} \tag{26}$$

The main result expressed by eq.26 is that at temperatures between T_g and T_c, the heat generation, at the beginning of the current diffusion, can be very high compared with the steady state value as shown in fig.5 for the ALEPH conductor. The total heat generation, as expressed by the eq. 25, was included in both the simple 1-D code and HEATING code. On performing 3-D thermal calculations using HEATING, care must be taken in evaluating how good is the used 1-D approximation of the current diffusion. For square conductors the current diffusion occurs in two dimensions, so that the 1-D approximation can overestimate the time dependent heat generation.

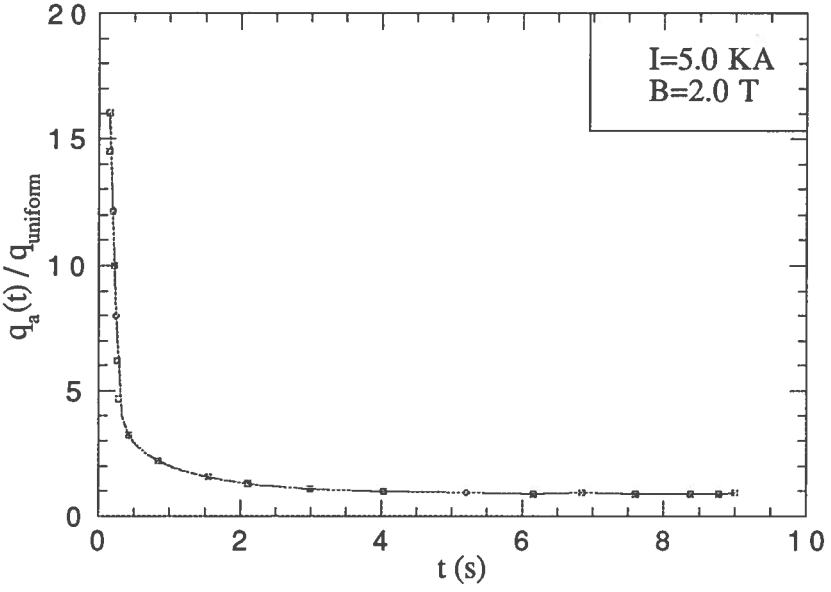

FIG. 5 - Time dependent heat generation in the ALEPH conductor due to the current diffusion effects.

4 - MPE CALCULATION IN A SIMPLE CASE

In order to carry on a first test of HEATING and to understand its capability to solve transient problems at low temperatures, where the specific heat and the thermal conductivity of solids have a strong dependence on temperature, we made a comparison of results obtained on a simple model by HEATING and by a 1-D code based on the CEP.

The model was a 1-D pure aluminium conductor of length 14 m, at initial temperature T = 4.22 K. The temperatures of the two ends are fixed at T = 4.22 K. Starting from time t = 0 s to time t = 0.01 s, a fixed energy is dissipated in a length of 1 cm in the middle of the conductor. We tried to find the energy amount that causes a quench. The current flowing in the conductor is 5 kA at the magnetic field of 2 T.

Figs. 6 and 8 show the temperature distribution calculated with the 1-D code at different times for two values of the disturbance. A disturbance of 0.34 Joule (fig.6) causes a temperature rise up to 7.1 K maximum, but no transition occurs. A disturbance of 0.35 Joule (Fig.8) causes instead a normal zone ($T>T_g$), not recoverable. Figs. 7 and 9 show the same situations from the point of view of the normal zone. In the first case (0.34 Joule disturbance) the normal zone saturates at a maximum of about 80 cm. In the second one (0.35 Joule) the normal zone propagates. The interesting feature of this simulation is that we can define a threshold value of the disturbance energy, causing a normal zone propagation.

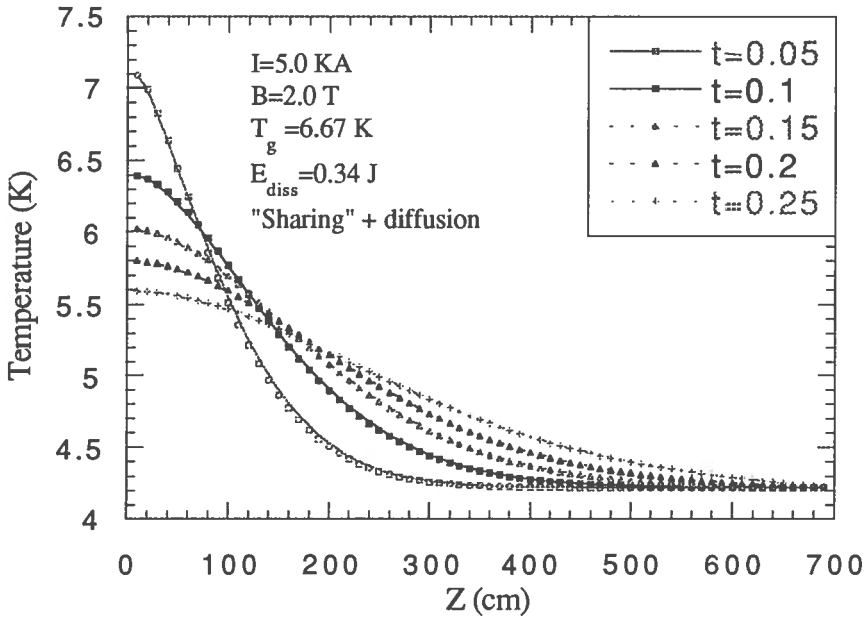

FIG. 6 - Development of a recoverable normal zone caused by a 0.34 Joule disturbance: temperature distributions

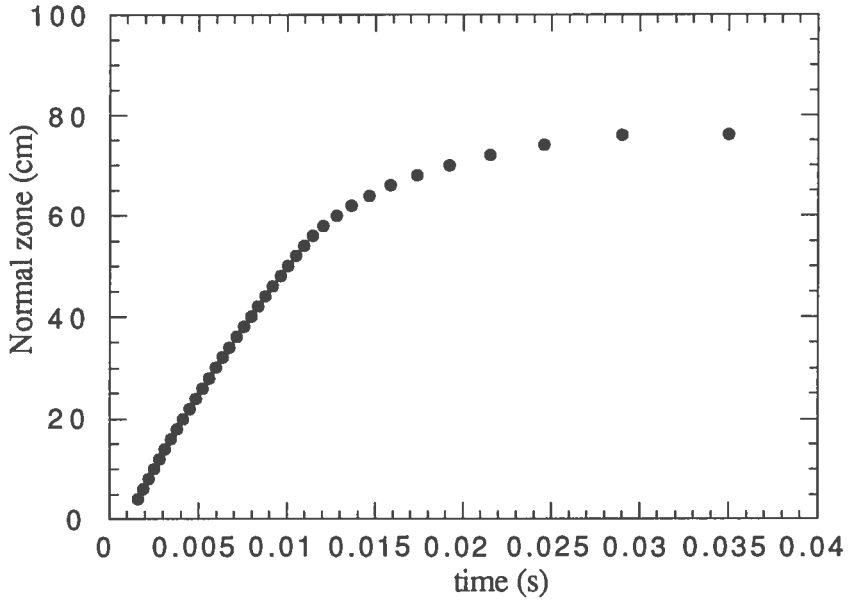

FIG. 7 - Development of a recoverable normal zone caused by a 0.34 Joule disturbance: normal zone evolution

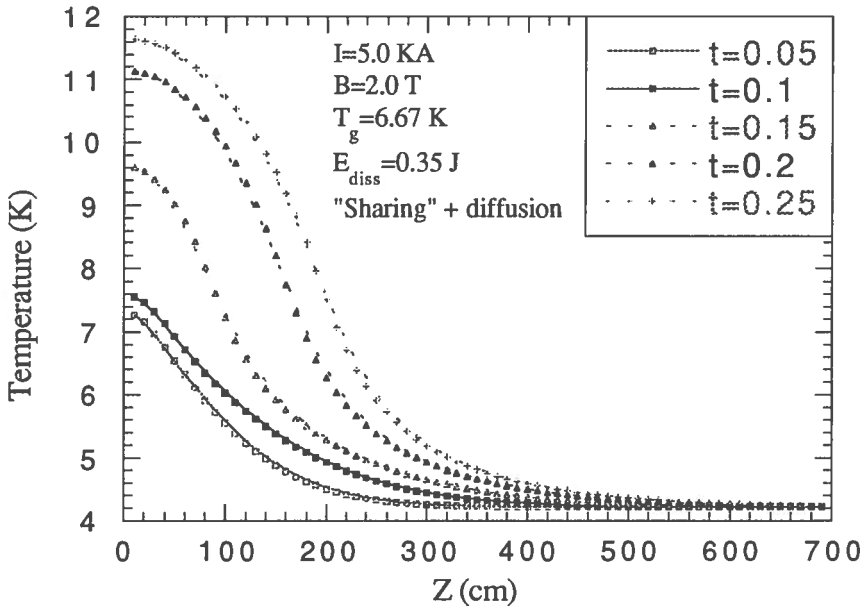

FIG. 8 - Development of a not recoverable normal zone caused by a 0.35 Joule disturbance: temperature distributions

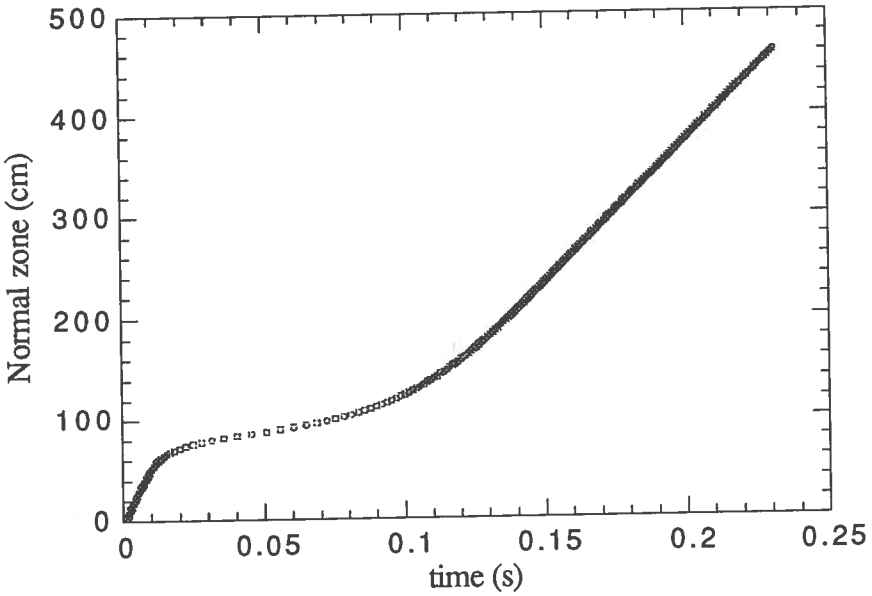

FIG. 9 - Development of a not recoverable normal zone caused by a 0.35 Joule disturbance: normal zone evolution

The same simulation was carried on using the HEATING code. The results are shown in Figs. 10.a and 10.b. In this case the energy release which does not cause a normal zone propagation is 0.33 Joule, while a disturbance of 0.34 Joule gives rise to a quench, a result close to one of the simple 1-D code. If the current diffusion is not taken into consideration, very different results are obtained. The *MPE* in this case has a value ranging from 0.88 Joule (HEATING) to 0.91 Joule (1-D code), i.e. 2.7 times the energy needed when the current diffusion effects take place.

A simulation was also carried on using the general purpose ANSYS code. In this case no external heat generation routine can be used. The S/C to normal transition is simulated through fictitious values of the electrical resistivity, so that there is no way to introduce the current diffusion effect. Table I shows a summary of results with and without the current diffusion effect obtained by the three codes.

The conclusions of this section are:

1- The 1-D and HEATING codes give the same results of *MPE* and *MPZ* for a simple 1-D model of ALEPH conductor. The *MPE* results of ANSYS code for the case with only current sharing are 50% lower. We think that the impossibility to handle a suitable heat generation routine leads to exclude the ANSYS code for stability calculations.

2- A threshold value of *MPE* can be defined within few percent approximation

3-The current diffusion effect has an important role in determining both *MPE* and *MPZ* , which for ALEPH conductor would be 2÷3 times higher if this effect does not take place.

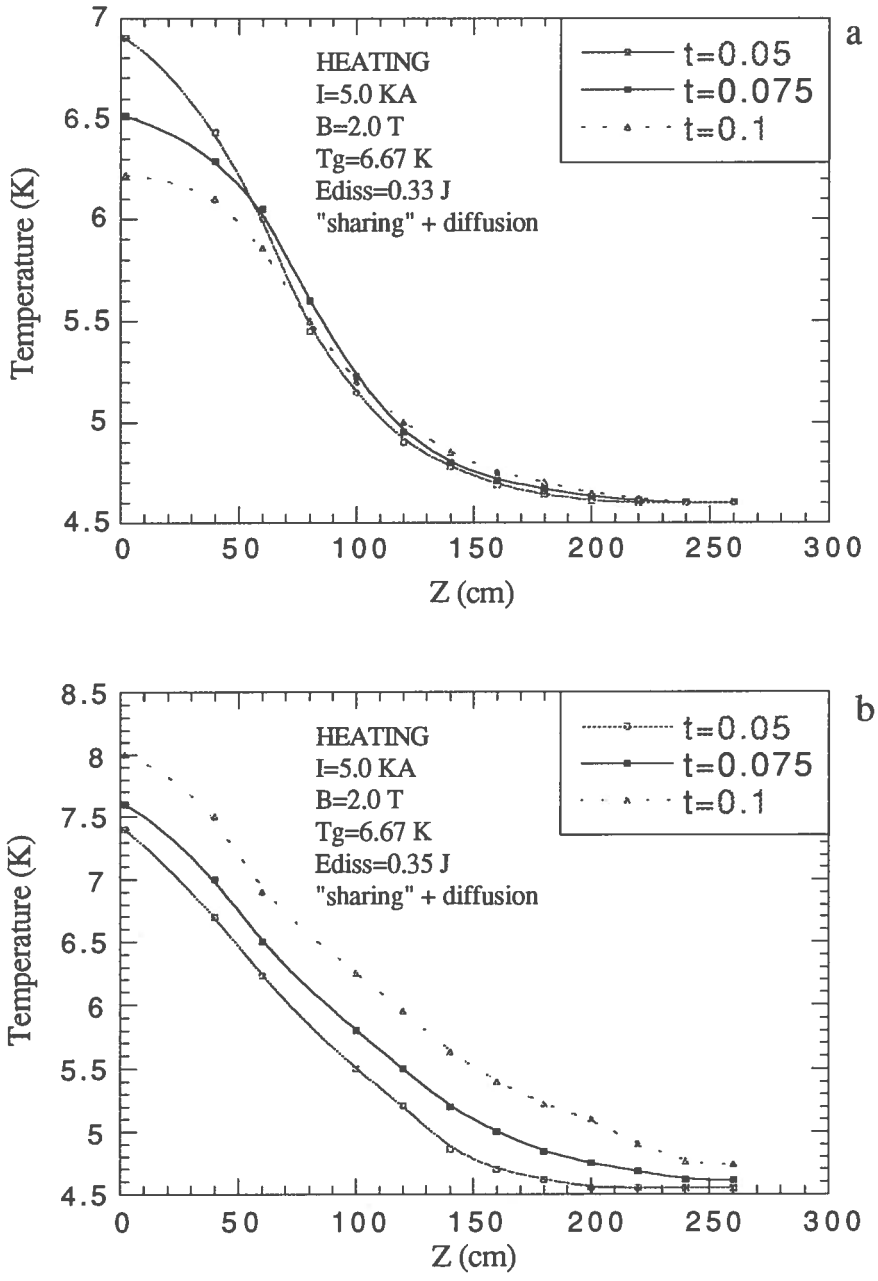

FIG .10 - HEATING code results a) Development of a normal zone caused by a 0.33 Joule disturbance; b) Normal zone propagation due to a 0.34 Joule disturbance.

TABLE I - Summary results of the simulations for the 1-D model

	Current-Sharing	Current-Sharing + Current diffusion
Model	ALEPH (1D)	ALEPH (1 D)
Current	5.0 KA	5.0 KA
Field	2.0 T	2.0 T
model length	14.0 m	14.0 m
Disturbance spread	0.01 m	0.01 m
Disturbance duration	0.01 s	0.01 s
MPE lower limit	0.91±0.01 J (1D code) 0.88±0.01 J (HEATING) 0.48±0.01(ANSYS)	0.34±0.01 J (1D code) 0.33±0.01 HEATING)
MPE upper limit	0.92±0.01 J (1D code) 0.90±0.01 J (HEATING) 0.50±0.01(ANSYS)	0.35±0.01 J (1D code) 0.34±0.01 J (HEATING)
MPZ	1.50±0.01 m (1D and HEATING) 1.40±0.01 m (ANSYS)	0.80±0.01m (1D and HEATING)
Quench velocity	3.6±0.1 m s^{-1}	13.0±0.1 ms^{-1}

5. - A SAMPLE HOLDER FOR CRITICAL CURRENT AND STABILITY MEASUREMENTS.

5.1. - Sample Holder

A sample holder was designed and constructed in order to carry on critical current and stability measurements in the MA.RI.S.A. magnet. This magnet can operate in two configuration: 6 T in 450 mm bore or 8 T in 330 mm bore. The sample holder was designed for 8T configuration and it is shown in fig. 11. We remark that the bore of the MA.RI.S.A. magnet only allows measurement to be carried out with the magnetic field parallel to the wide face of the conductor. Fig. 11 shows the sample holder adapted for the ALEPH conductor.

The conductor, insulated by a kapton strip, is placed in an aluminium alloy (6061) support ring, which both holds the outward directed magnetic forces and is the medium to indirectly cool the sample (when the LHe level is kept well below the conductor).

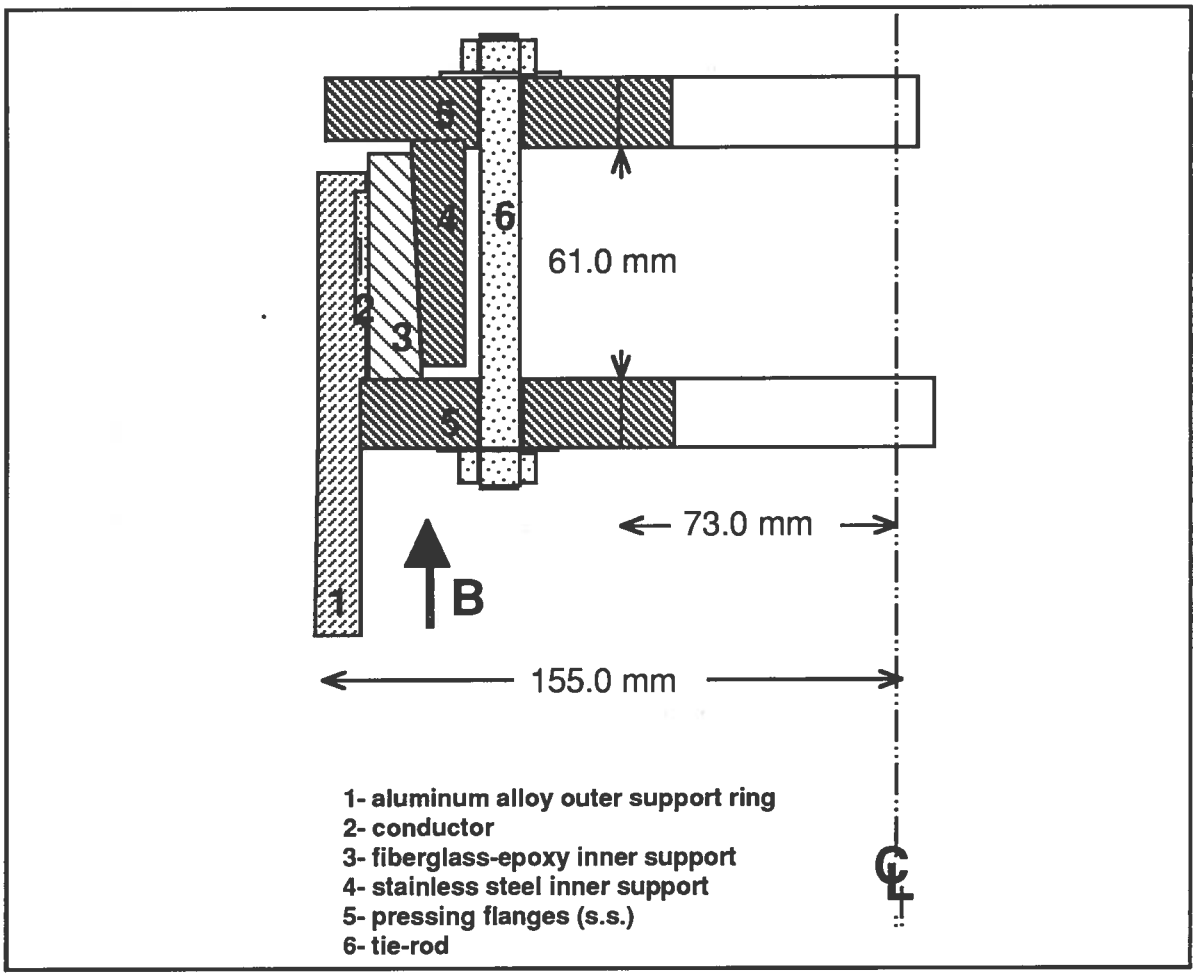

FIG. 11 - Sample holder for electrical measurement on ALEPH conductor

The conductor is pressed against the outer support using an internal conical open fiberglass-epoxy ring, stressed by a two stainless steel flanges+conical ring system, as shown in fig 11.

5.2 - Transformer method

The sample is fed using a transformer[10] having the background magnet as primary coil and the sample as secondary coil. This method allows large current (60 kA) to be circulated inside the sample as required for CMS and ATLAS prototype conductors. Fig. 12 shows a schematic of the transformer method.

Let be $\Phi(t)$ the time dependent magnet flux collected by the sample; the equation for the current I(t) in the sample is:

$$\dot{\Phi}(t) = L_S \dot{I}(t) + R_G I(t) \qquad (27)$$

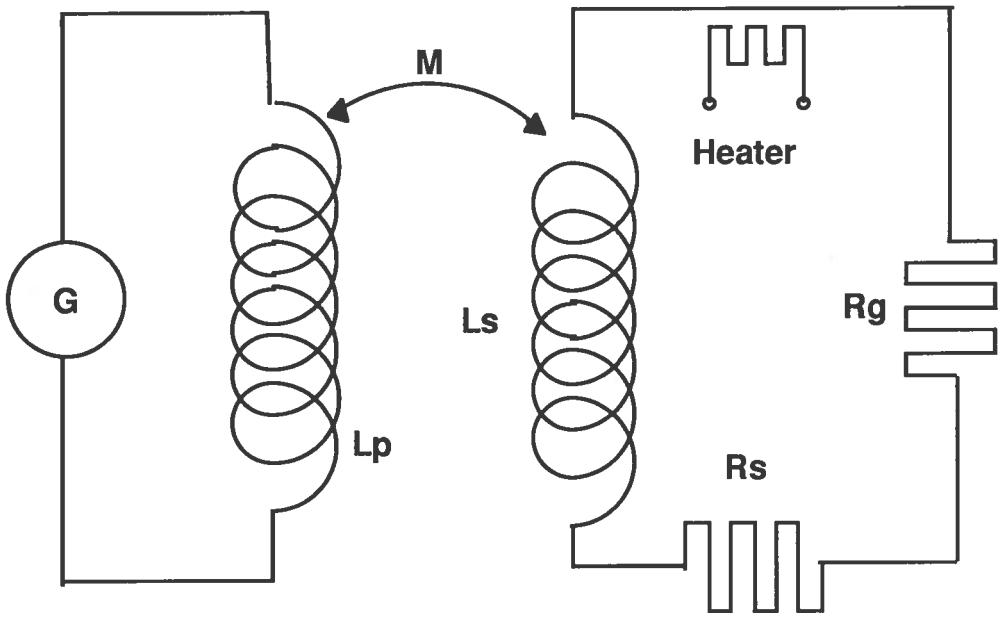

FIG. 12 - Schematic of transformer method. G - Magnet power supply; L_p - Background magnet inductance (Primary winding); L_S - Sample inductance (Secondary winding); M - Mutual inductance; R_S - Sample resistance (R_S=0 if superconducting) ; R_g - Joint resistance

Where L_S is the sample inductance and R_G the joint inductance. If $\dot{\Phi}(t)$ = cost., the solution of eq. 27 simply is:

$$I(t) = \dot{\Phi}(t)\frac{\tau}{L_S}\left(1 - e^{-\frac{t}{\tau}}\right) \tag{28}$$

where τ is the time constant defined by $\tau = \frac{L_S}{R_G}$. Derivating eq. 28 and supposing to be in the limit $t \ll \tau$ s, we obtain :

$$\dot{I}(t) = \frac{\dot{\Phi}(t)}{L_S}, \tag{29}$$

so that

$$I(t) - I(0) = [\Phi(t) - \Phi(0)]\frac{1}{L_S} \tag{30}$$

Writing the magnetic flux as function of the background magnet current $I_{mag}(t)$:

$$\Phi(t) = MI_{mag} = k\sqrt{L_s L_p}\, I_{mag}, \tag{31}$$

where M is the mutual inductance, k the mutual inductance coefficient and L_P the magnet inductance, from Eqs. 30 and 31 we find the Current Transformer Ratio:

$$\alpha = \frac{\Delta I_{sample}}{\Delta I_{mag}} = k\sqrt{\frac{L_P}{L_S}} \qquad (32)$$

In our case the sample of ALEPH conductor has an inductance $L_S = 8.81\ 10^{-7}$ Henry and the mutual inductance is $M = 6.45\ 10^{-4}$ Henry. The measured magnet inductance is 9 H so that the Current Transformer Ratio is $\alpha = 732$, i.e. for 1 A of the magnet current variation, a current of 732 A is induced in the sample.

The current in the sample is measured through one or more Hall probes, which detect only the self field as shown in fig. 13. In this measurement it is very important not to detect the background magnetic field, which could give an extra signal much higher than the self field signal.

The voltage V_{EF} can be written as:

$$V_{EF} = a_1\dot{\Phi}(t) - a_2 L_S \dot{I}(t) - \left(\frac{R_S}{2} + R_G\right) I(t) \qquad (33)$$

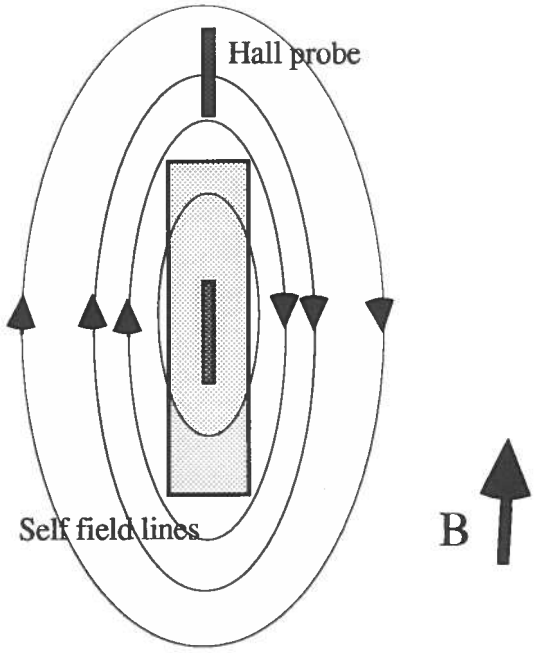

Fig. 13 - Self field measured using a Hall probe

The voltage taps should be carefully positioned. In fig 14 a top view of the sample holder is shown. The dashed lines represent the wires for the voltage reading between two points placed at 180 degrees.

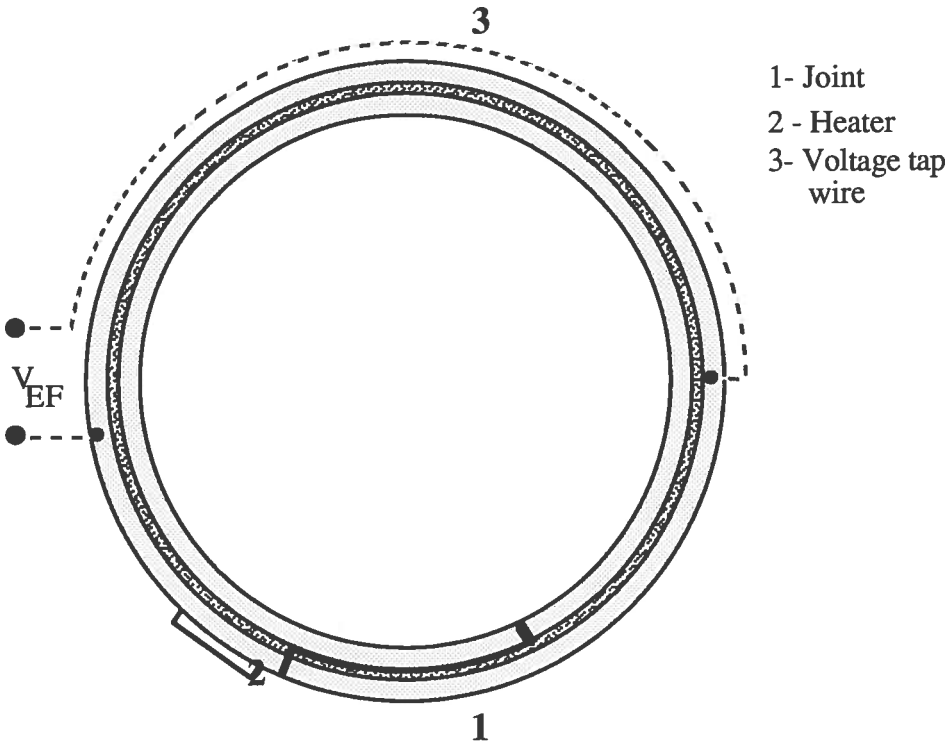

FIG. 14 - Top view of the sample, with the connections for the voltage reading

The coupling coefficients a_1 e a_2 depend on how good the wire 3 in fig. 14 is magnetically coupled to the half sample not containing the joint. In the limit of perfect coupling, i.e. $a_1=a_2=1$, using eq. 27, eq. 33 becomes:

$$V_{EF} = \frac{1}{2} R_S I(t) \qquad (34)$$

Measuring the current I(t), using the Hall probe, and the voltage V_{EF}, we obtain the sample resistance $R_S(I)$. The voltage V_{EF} is also used for stability measurements as shown in later sections.

5.3. - Joint Development

In order to carry out critical current and stability measurements with the transformer method, the joint resistance should be as low as possible. A maximum value of $R_G=5\ 10^{-9}\ \Omega$ can be acceptable. For higher value of R_G the time constant for the current decay $\tau=L_s/R_g$ becomes too short (170 s) with relation to the time needed to charge the sample. The joint was made removing the aluminium at one side of the sample ends, as shown in fig. 15, for a length of about 200 mm (a twist pitch); then several attempts to solder the overlapped ends were made.

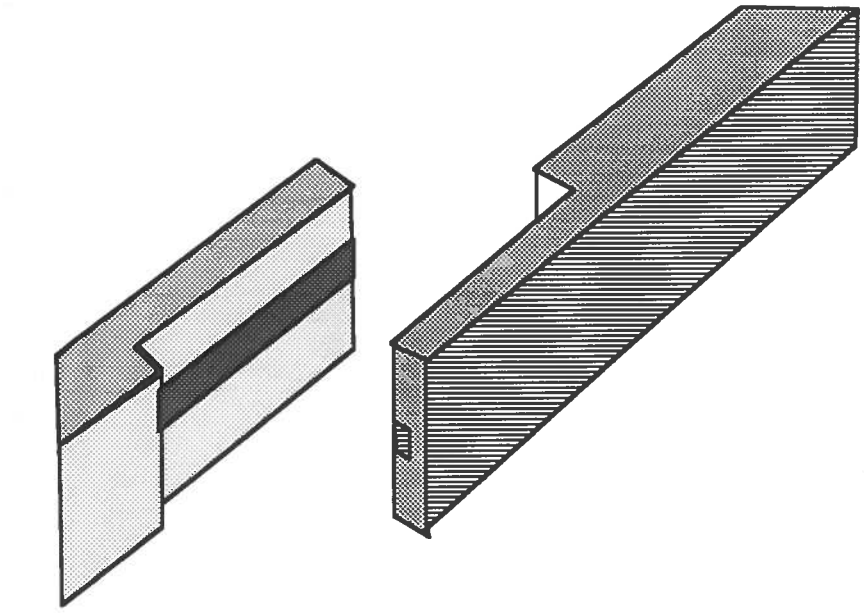

FIG. 15 - The two ends of the sample are machined and overlapped

No satisfactory results were obtained using the following two techniques:

1- The surfaces to be overlapped were mechanically cleaned. Indium was inserted between them, and then a pressure was applied . The best joint resistance was $R_G=14\ n\Omega$ at T=4.2 K.

2- The surfaces were covered by a metal (copper or silver or tin) with an electrochemical process. Then a soldering with indium or tin-lead alloy was tried. The surface resulted damaged and dirty .

Encouraging results were obtained covering the surface, heated at 155 °C, with a melted indium layer whilst using a special aluminium soldering flux to allow a good adhesion of the indium to the aluminium. After the indium covering, the sample ends were pressed and heated in furnace at 140 °C. The last cycle was repeated 3 times, until the two ends came in the best contact.

The joint resistance was measured through the time constant measurements at temperature T=4.2 K and in the magnetic field range 0÷4.5 T. The results are shown in fig. 16.

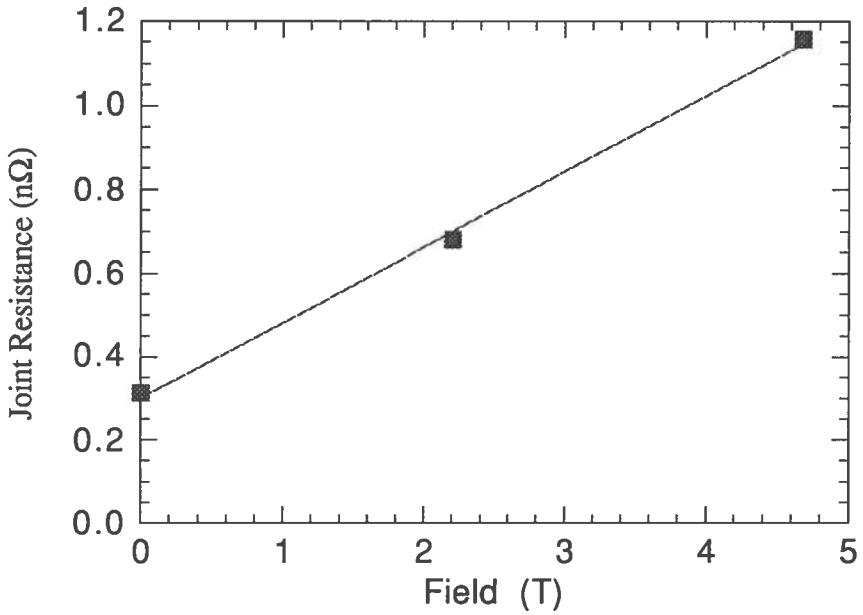

FIG. 16 - Joint resistance as function of the magnetic field

6. - CRITICAL CURRENT MEASUREMENT

The critical current is measured using the set up shown in fig. 17. The magnet generating the background field is charged a fixed field keeping the sample in the normal state using a heater. The heater is turned off, so that the sample goes to be fully superconducting. The current of the background magnet is linearly lowered, causing a linear current ramp in the sample. The voltage V_{EF} and the Hall probe signal are monitored obtaining a current voltage characteristic as shown in fig. 18. Since the coupling constant a_1 and a_2 are lightly different from the unity, an inductive voltage is detected during the charge of the sample. When the voltage V_{EF} increases due to the S/C to normal transition, the background field variation is stopped, so that no further current is induced in the sample. The current in the sample slowly decreases allowing a measurement of V-I characteristic at fixed field. The critical current is defined by the resistive criterion $\rho_n=10^{-14}$ Ωm.

Fig. 19 shows a measured V-I characteristic of ALEPH conductor at 4.2 T magnetic field. In Fig.20 the same data are displayed in logI-logV graph. In the figure the line at constant resistivity $\rho_n=10^{-14}$ Ω m is also shown. The current of the intersection point is the critical current. The voltage has a power dependence on the current $V \propto I^n$, with n=45. Fig.21 shows

the critical current Vs the magnetic field. Two curves are displayed depending on which field is considered to be applied to the sample: the external field or the peak field, i.e. the external plus the self field. For comparison with results of other laboratories the results with the peak field should be held.

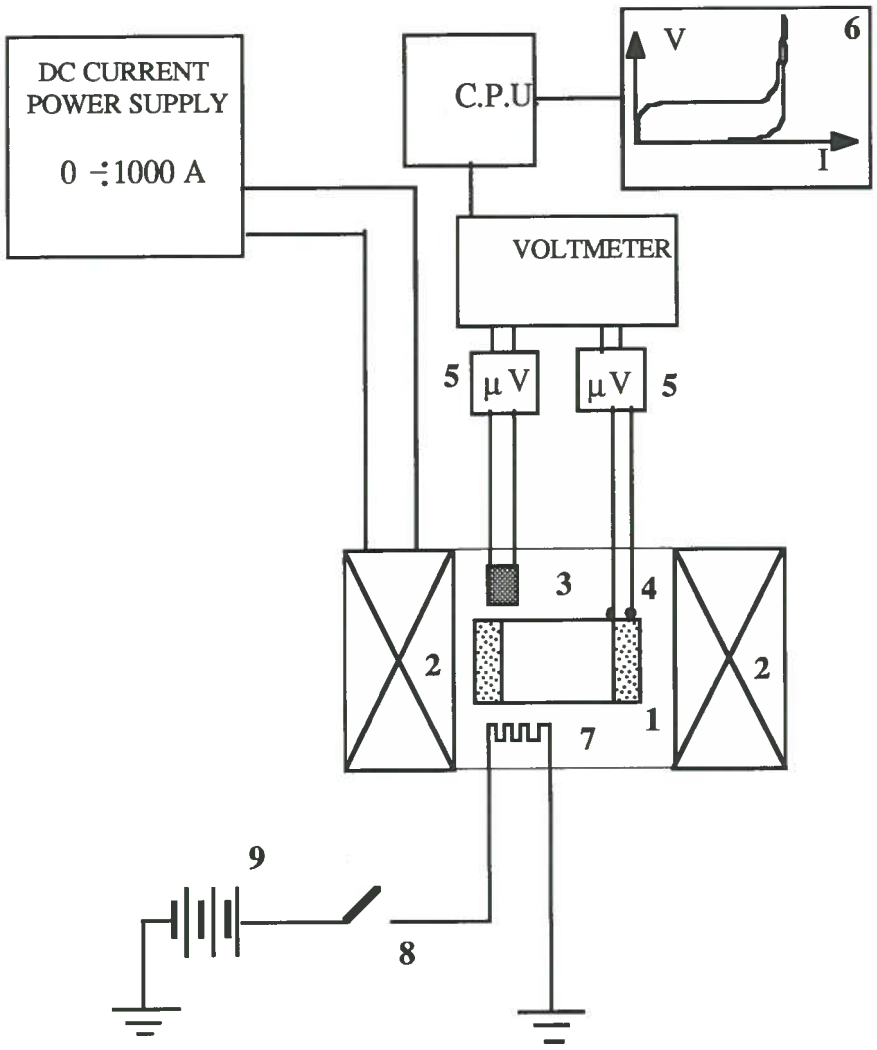

1 Sample
2 Background magnet (MA.RI.S.A.)
3 Hall probe
4 Voltage taps
5 Keythley analog microvoltmeter
6 Plotter xy HP
7 Heater - 20 Ω
8 Switch
9 Heater Power supply

FIG. 17 - Critical current measurement set-up

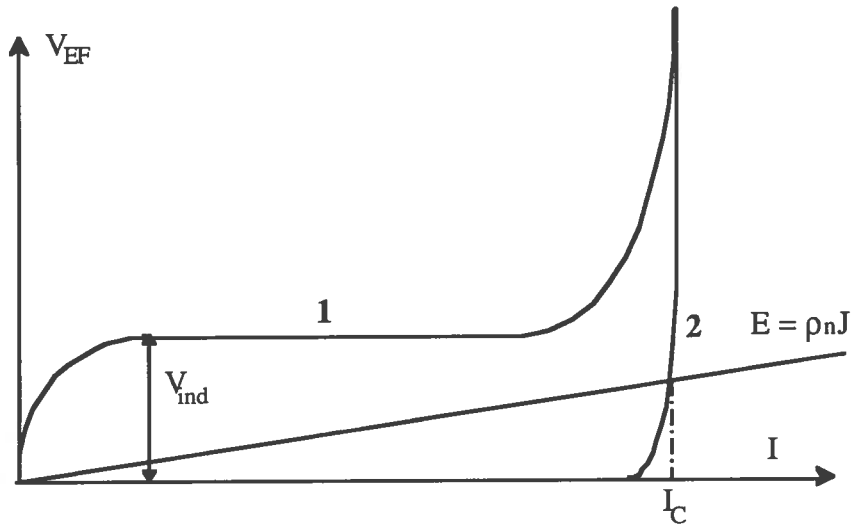

FIG. 18 - Typical V-I characteristics: 1- The sample is charged discharging the background magnet ; a low inductive voltage is detected. 2- The sample current decays allowing a measurement to be carried out at fixed magnetic field

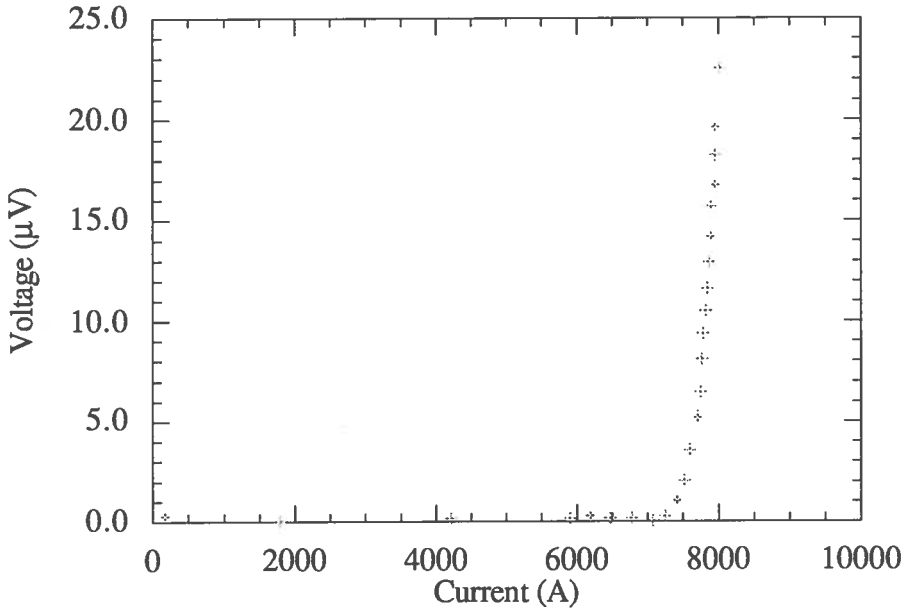

FIG. 19.- VI characteristic of ALEPH conductor at constant applied field B=4.12 T.

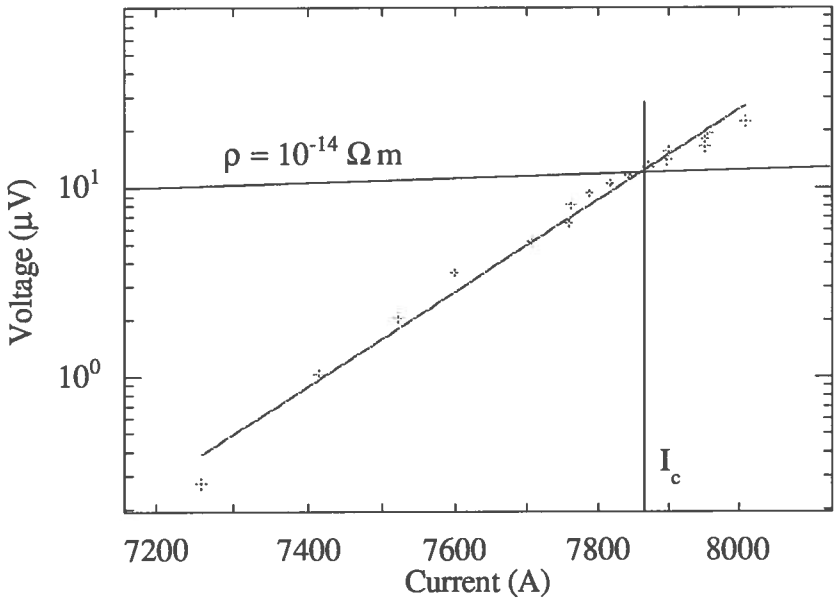

FIG. 20 - The data of fig.19 in log scales . The intersection of the data power fit (n=45) and the constant resistivity line gives the critical current.

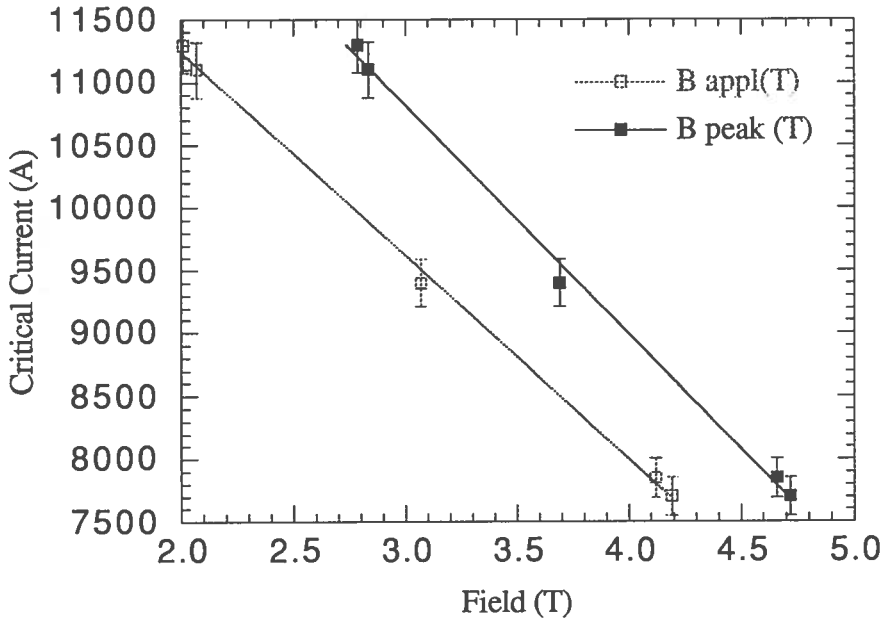

FIG.21 - Critical current of ALEPH conductor measured with the transformer method as function of the external and the peak magnetic field

7. - STABILITY MEASUREMENT

In order to perform stability measurement we used the set up shown in fig.22. The set up is similar to the one for critical current measurement except the part regarding the disturbance generation. In this case we need to dissipate a well determined energy close to the sample. A pulse generator (9) was used, to have square pulses of fixed amplitude and duration.

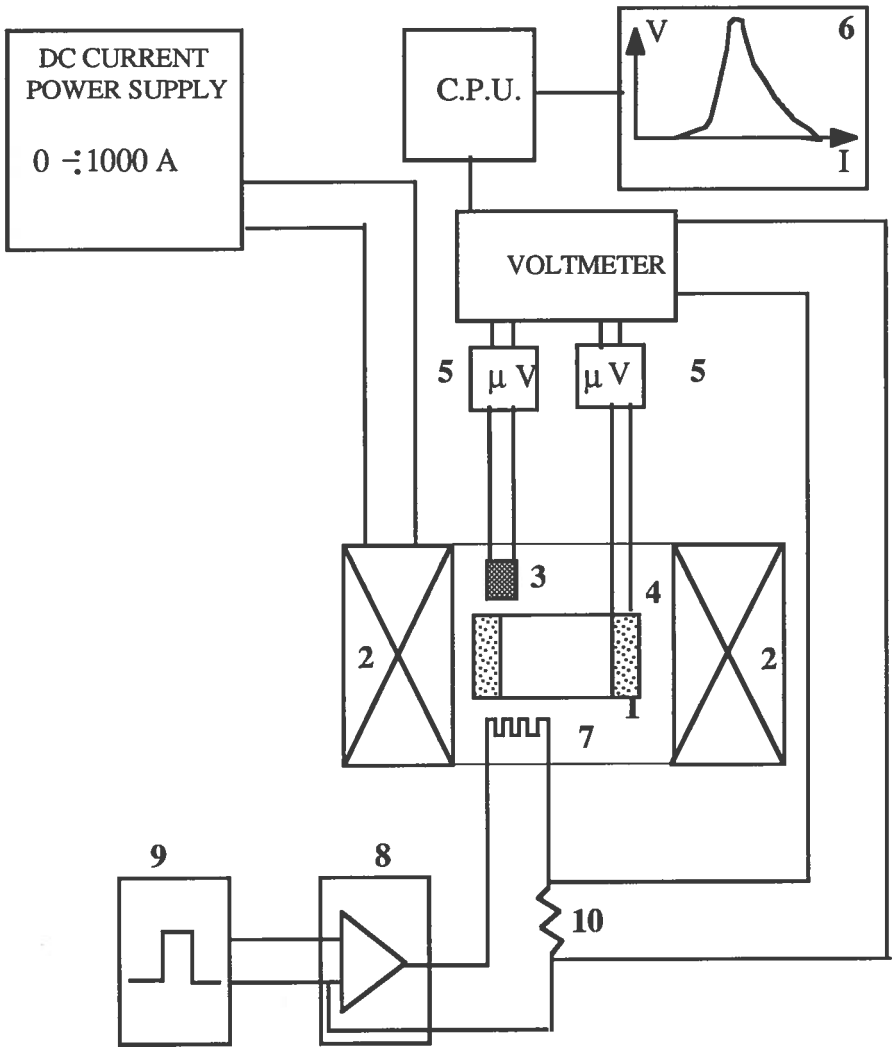

1 Sample
2 Background magnet
3 Hall probe
4 Voltage taps
5 Analog micro-voltmeters
6 Plotter xy
7 Heater
8 Four quadrant amplifier (200 W)
9 Pulse generator
10 Heater current shunt

FIG.20 - Schematic of stability measurements set up.

The heater resistance is 13 Ω , since the maximum current which can be given is I=2.5 A, the maximum power is $W= RI^2= 81.3$ Watt . The disturbance energy is then varied changing the duration t^* of the pulse. The measurements were carried on giving a disturbance and monitoring the voltage V_{EF} Vs the current. The formation of recoverable normal zone gives rise to a small voltage related to a low current decay. A quench causes high voltage and a big variation of the current in the sample.

Fig.23 shows the V-I characteristic measured with a pulse duration $t^*= 70$ ms, which corresponds to an energy of $E_{diss}= 5.7$ J. The initial current in the sample is $I_{Si}= 5800$ A, at a field of B=2.0 T (the working values for the ALEPH conductor); the graph reports the voltage drop V_{EF}, as a function of the current decay in the sample I_S-I_{Si}.

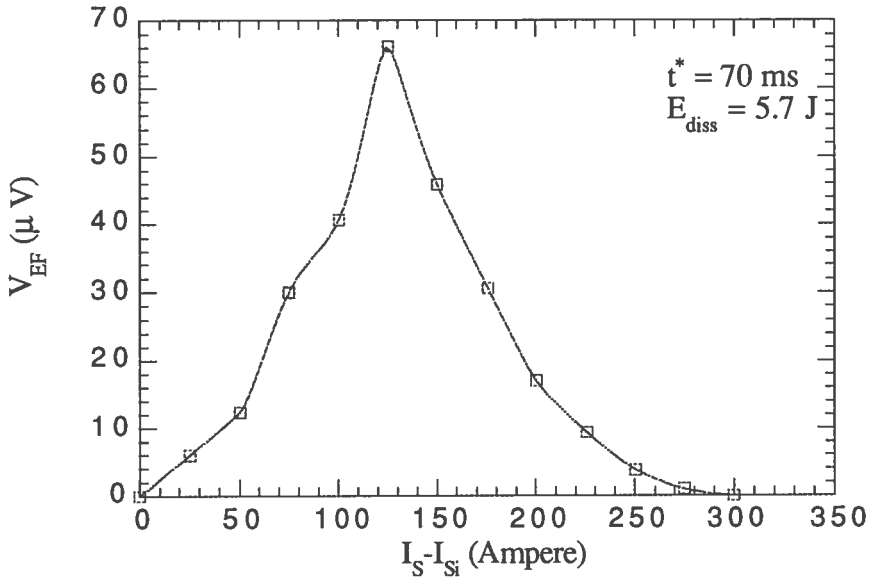

Fig.23 - V-I characteristic for a disturbance of 5.7 J

A weak voltage represents the forming of a little normal zone inside the conductor, the current decays due to the dissipation and, after approximately 1s, the sample recovers at a current value (320±25 A) lower than the initial value. The V-I characteristic demonstrates the forming inside the conductor of stable normal zones, which quickly shrink to recover the superconducting state. Increasing the disturbance energy to a pulse of $t^*= 80$ ms, i.e. $E_{diss}=6.5$ J, a great difference in the behaviour of the conductor has been measured, as shown in fig.24. The substantial differences concern both the voltage and the value of the current decay: the disturbance energy is enough to give rise to an unstable regime, with the propagation of the normal zone to the whole sample. The current recovery occurs at 1800 A lower than the initial current and more than 2 s after the beginning of the disturbance.

So the limit energy to guarantee stability to the sample, or MPE, has been measured to lie between 5.7 J and 6.5 J.

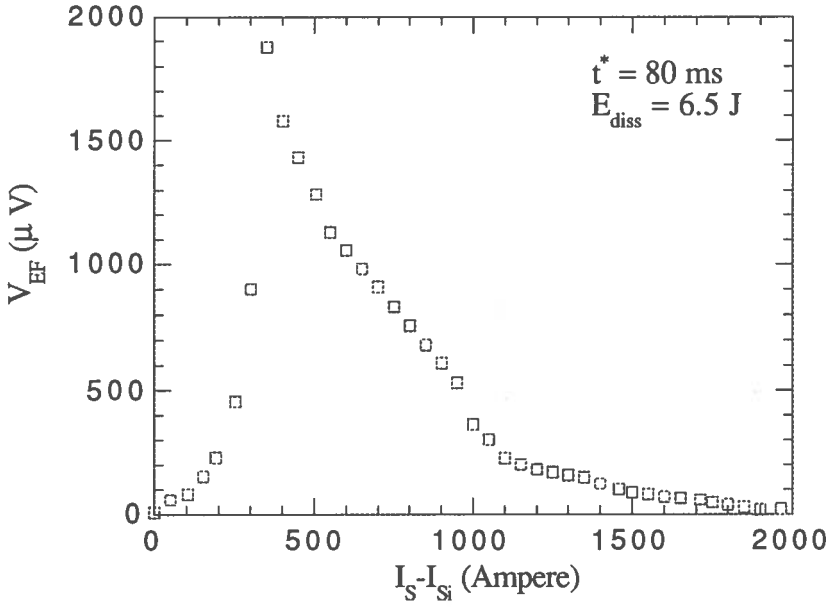

FIG. 24 - V-I characteristic for a disturbance of 6.5J

8. - COMPARISON BETWEEN RESULTS AND SIMULATIONS

Let us observe that the measured *MPE* is higher than the calculated value by 1-D cold-end simulations; this means that the 1-D calculations allow to understand the general behaviour of a conductor subject to a heat disturbance, while in a real situation the indirect cooling on plays an important role on stability.

In order to compare experimental results with stability simulations a 3-D model using the HEATING code has been developed. The heat generation routine was modified to account the current decay during the normal zone evolution. This is a peculiarity of the transformer method. The used model is shown in fig.25: the ALEPH conductor, 1m length, is enclosed in an aluminium alloy ring . Between the conductor and the alloy ring a thin insulating layer 0.1 mm thick is interposed. This layer simulates the kapton electrical insulation of the conductor.

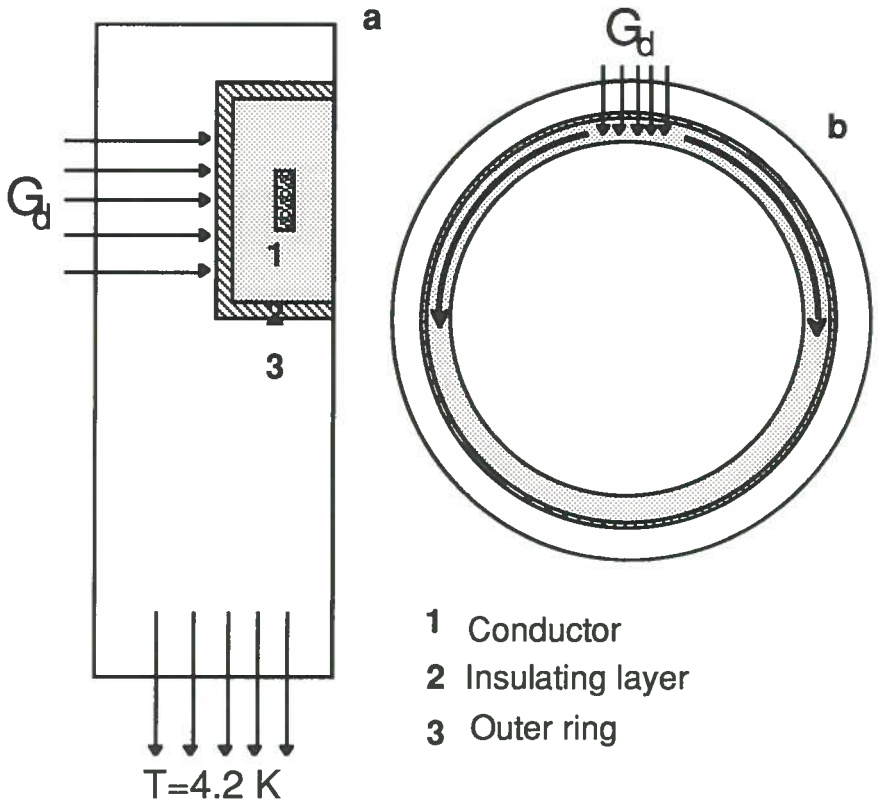

FIG. 25 - Model of the sample holder : a) Cross section b) Top view

The cooling occurs through the thermal exchange with a liquid helium bath, at the same level of the lower border of the aluminium alloy ring. In the real sample holder, the conductor is in contact with a fiberglass-epoxy ring at the inner radius . Since the heat exchange through the fiberglass epoxy is very poor, we completely neglected to put in the model this part as well as the supporting stainless steel flanges. The heater is represented by an heat generation G_d in a small part of the conductor (1 cm length). The simulation were carried on with the *CEP* technique, which gives the best results but requires long time: for a 4 seconds simulation 36 h of CPU on ALPHA-VAX are needed. This long time is mainly due to the HEATING "user supplied subroutine", which calculates the heat generation taking into consideration the temperature dependence of the electrical and thermal properties of the involved materials. The time step calculated according to eq.6 was $3\ 10^{-7}$ s . Faster , but less accurate calculations could be performed using the Levy's technique or some implicit procedures. Since in our set up the disturbance causes a current decay, with the result of a recovery of the superconducting state at some currents lower than the initial one, we restricted our attention on the recovery current. Fig 26 shows the temperature distribution along half a conductor due to a 5.7 Joule disturbance. The superconducting state is restored in 0.5 s. Fig.27 shows the current decay due to the normal zone evolution. The disturbance does not seem to strongly affect the current which is lowered of 200 A.

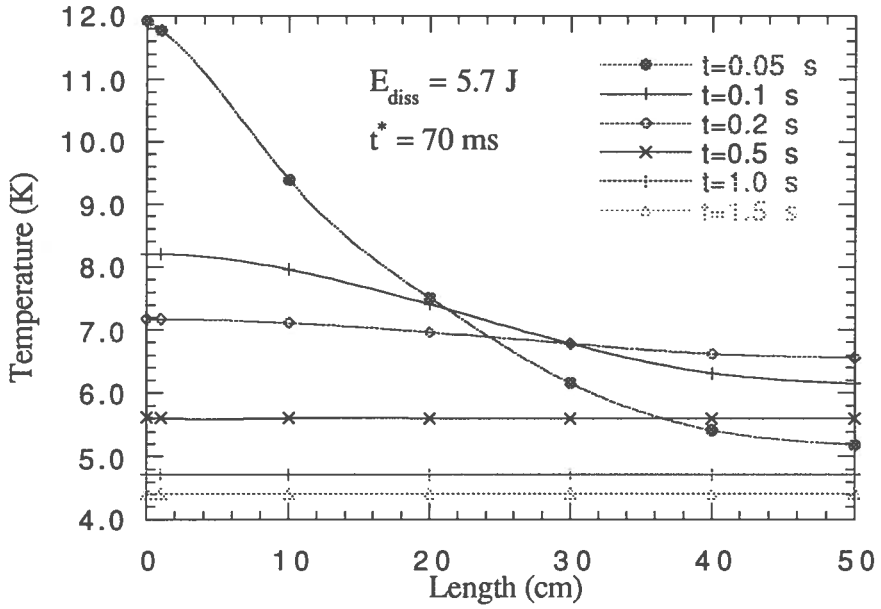

FIG. 26 - : Calculated temperature profiles along half the sample after a disturbance of 5.7 J

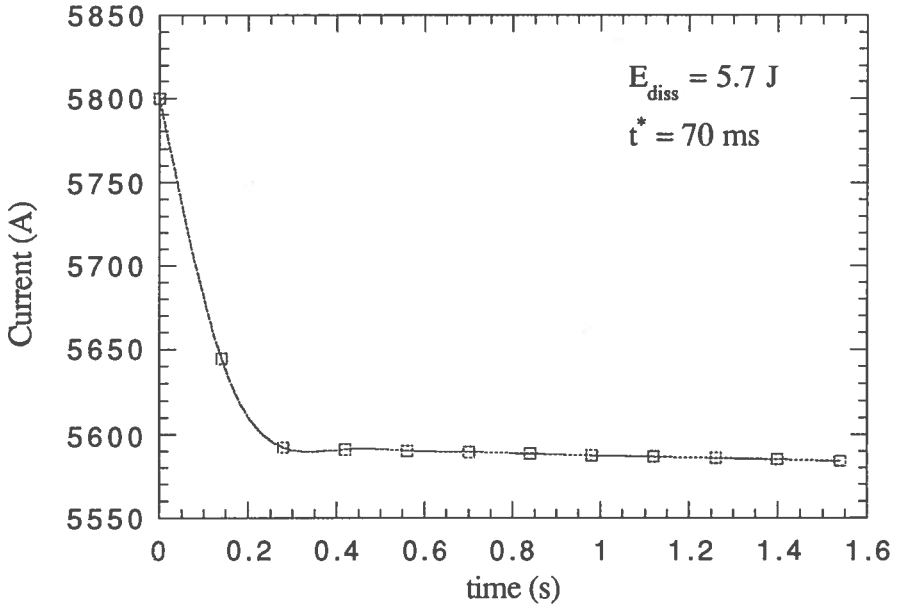

FIG.27 - Calculated current decay in the sample due to a disturbance of 5.7 J

If a disturbance of 6.5 Joule is applied, the response of the conductor dramatically changes. In this case for a time of 1.5 s the whole conductor remains in the normal state (Fig.28) at

temperatures T>6.67 K and the current decays of 1100 A (Fig.29). Simulations with no current diffusion effects were performed too. In this case a 6.5 J disturbance causes a current decay of 600 A,.

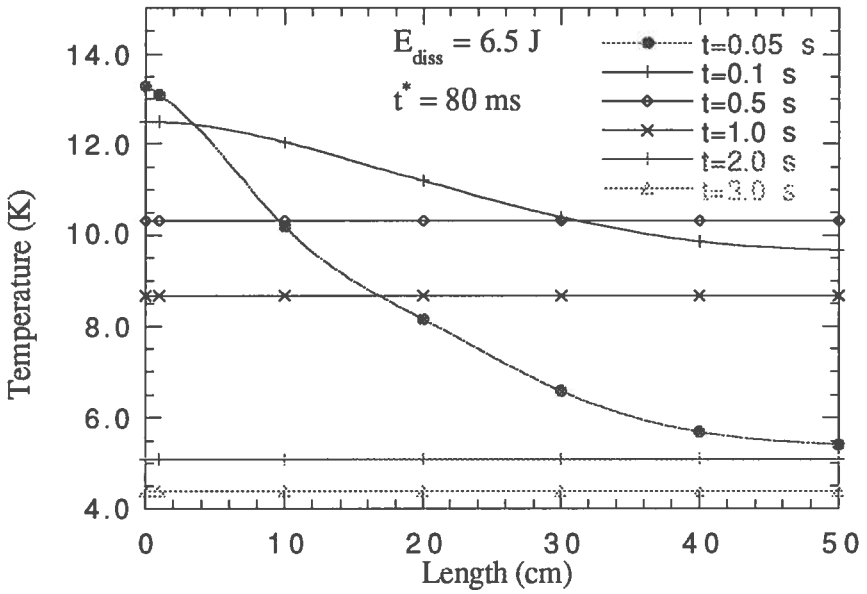

FIG. 28 - Calculated temperature profiles along half the sample after a disturbance of 6.5 J

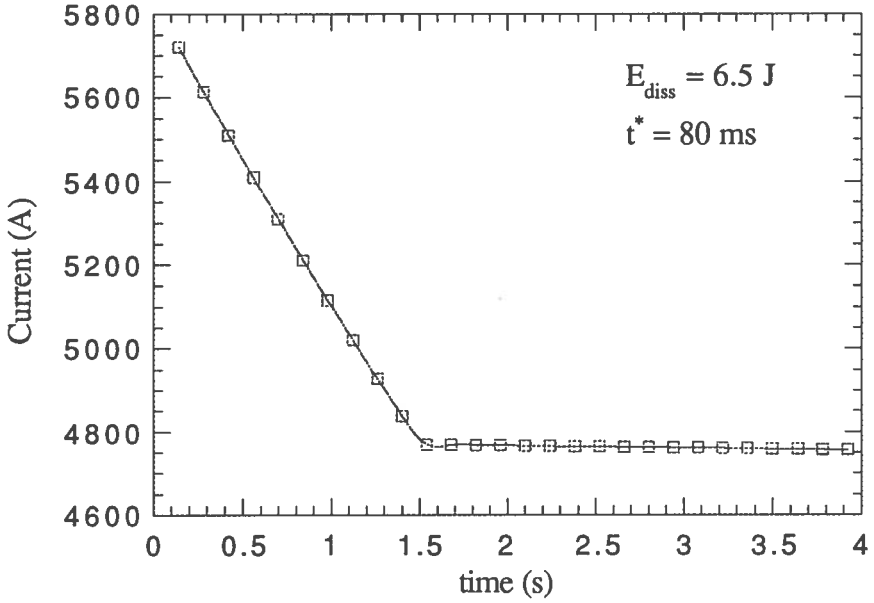

FIG.29 - Calculated current decay in the sample due to a disturbance of 6.5 J

The conclusion of the stability studies section is that the developed models seem to account the experimental results. The measured stability margin of *MPE* lies between 5.7 and 6.5 Joule, as calculated by HEATING with our model. The measured current decay in stable and unstable

situations are 320 A and 1800 A, while the calculated values are 200 A and 1100 A, i.e. not so far from an acceptable agreement. If the current diffusion effects are not considered, the results of simulations do not agree with the experimental one.

9. - CONCLUSIONS

The results obtained can be summarised as follows:

1- A sample holder for critical current measurements of aluminium stabilised conductors has been developed and tested. The studied techniques will be used to develop the sample holders for the non-reinforced prototype conductors already ordered by the CERN.

2- Different numerical codes were tested in order to understand their application in stability calculations. A modified version of HEATING code seems to be an interesting tool for this purpose.

3- The sample holder for critical current measurements can be also used for stability measurements, if the current decay in the sample, due to a given disturbance, is taken into consideration as stability parameter

4- The current diffusion effects were proved to have an important role in determining the stability of aluminium stabilised conductors.

REFERENCES

1- ATLAS, *Letter of Intent*, CERN 1992

2 - CMS, *Letter of Intent,* CERN 1992

3 - D.U. Von Rosemberg, *Methods for the Numerical Solution of Partial Differential Equations*, American Elsevier Publishing Company, N.Y. 1969

4- HEATING 7.2b user manual, RSIC PERIPHERAL SHIELDING ROUTINE COLLECTION PSR199, Oak Ridge National Laboratory, March 1993

5 - S.Levy, *General Electric*, 68-c-282, Schenectady, N.Y. 1968

6 - J.Crank, P.Nicolson, *Proc.Cam.Philos.Soc.*, 43,1947

7 - M.N.Wilson, *Superconducting Magnets,* Clarendon Press, Oxford,1983

8 - E.W.Collings, *Applied superconductivity, Metallurgy, and Physics of Titanium Alloys,* Plenum Press, N.Y., 1986

9- A.Lee, R.H.Wands and R.W.Fast, *Cryogenics,* Vol32, No10, 863-866, 1992

10- P.Fabbricatore, R.Musenich, and R.Parodi, *Nucl.Instr. and Methods* A 302, 27-35, 1991